

ACS WFC & HRC field-dependent PSF variations due to optical and charge diffusion effects

John Krist
June 25, 2003

ABSTRACT

The ACS point spread function remains fairly stable over its field of view, compared to the PSFs in WFPC2 or STIS. However, ACS/WFC PSF core width and ellipticity variations are large enough to be of concern to those undertaking very small aperture photometry or measuring small, bright-nucleus galaxy ellipticities. The lower limit to the PSF width is demonstrated to be set by CCD charge diffusion, which is field-dependent due to thickness variations in the detectors; the upper limit is set by elongation of the PSF due to the combination of field-dependent astigmatism and defocus, and time-dependent defocus. The aberration and charge diffusion variations have been characterized and are implemented in the Tiny Tim PSF modelling software (version 6.1 and later). Asymmetry variations due to coma, astigmatism, and defocus are explored using Tiny Tim models. The relationship between CCD thickness and flat field patterns is also discussed.

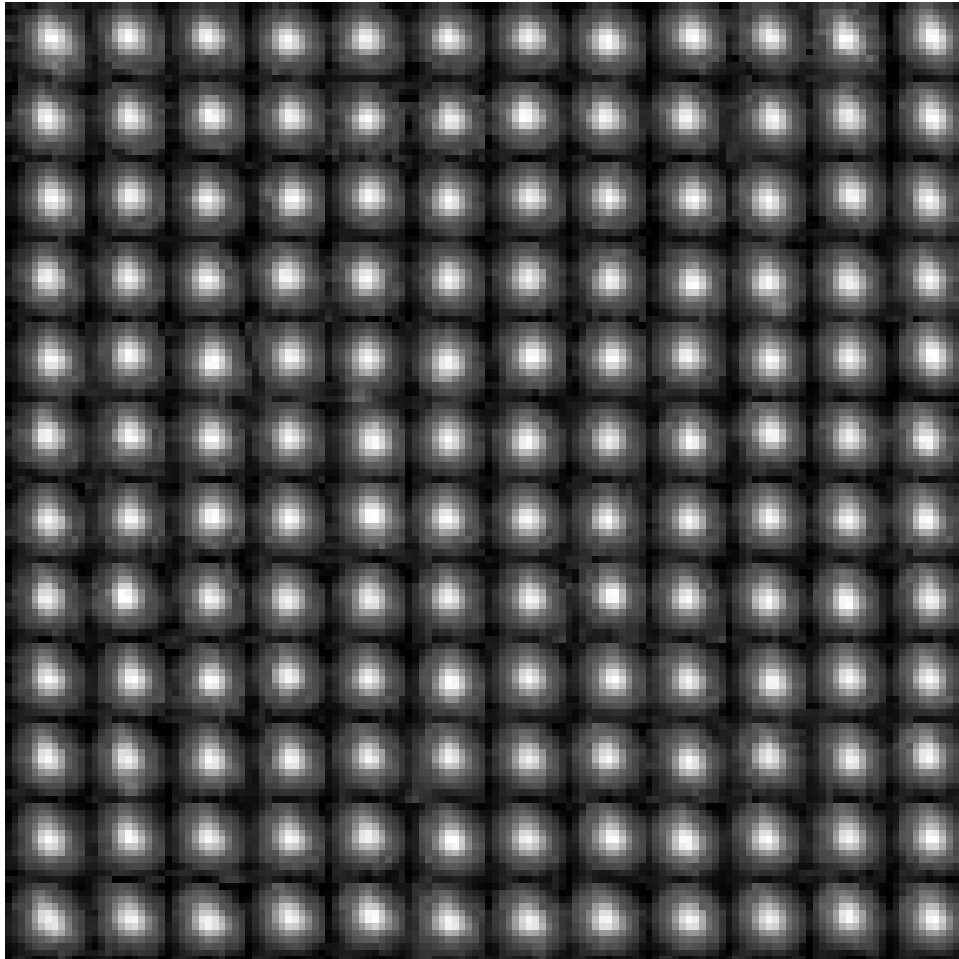
Introduction

Some HST science programs depend on the stability of the point spread function (PSF) and are sensitive to changes in its structure over the field of view. In cosmic shear studies, for example, measurement of galaxy ellipticity may be influenced by the intrinsic ellipticity of the PSF for small galaxies with bright cores. Crowded field stellar photometry using very small apertures (1-2 pixels) can also be impacted by variations in the shape and width

of the PSF over the field, which can alter encircled energy curves and thus aperture corrections.

In general, PSF field-dependent variations in ACS are less than in the other HST cameras. This is due to the relatively simple ACS optics (no additional obscurations) and optimization for imaging (in contrast to STIS, which is optimized for spectroscopy). However, due to optical and detector effects, the ACS PSF does vary over the field, most notably in the WFC (Figure 1), and the changes may be important for some science programs.

Figure 1: WFC F550M PSFs located at their relative field positions.



Causes of PSF Field-Dependent Variations

Aberrations

The primary source of PSF asymmetry variations over the field is the combination of defocus, coma, and astigmatism. These are present in practically every optical system due to design constraints and fabrication errors. Any aberration will reduce the flux within the core of the PSF and distribute it into the wings, degrading the encircled energy within a small aperture. Where the light gets redistributed depends upon the aberration.

Defocus is often apparent in wide-field systems because the focal plane is usually a curved surface. Its primary effect is the symmetrical redistribution of light from the core into the adjacent diffraction rings, reducing contrast and sharpness. Small focus changes, however, do not significantly alter the width of the PSF core. Optically-induced defocus usually increases away from the center of the camera, but sometimes tilt or warping of the detector can create larger variations over the field.

Coma skews the core of the PSF to one side, which can alter centroid measurements. Depending on the instrument, the amount of coma can either increase away from the optical center of the camera or slope across the field.

Astigmatism elongates the PSF, as if it were stretched along one axis. Its effects are strongly dependent on defocus. The angle of the major axis of an astigmatic PSF will switch 90° through focus. Astigmatism usually increases away from the camera optical center, so that PSFs at the center are generally symmetrical but those in the corners are elongated.

Another optical artifact, geometric distortion, is not really a wavefront aberration but rather a sky-to-detector projection effect that can alter the scale over the field of view. Distortion is discussed in detail in other documents (see the Instrument Handbook or Meurer et al. 2002). Geometrical distortion in ACS skews the imaged PSF, slightly elongating the core in a manner that somewhat resembles astigmatism.

Internal Obscurations

WFPC2 (and WF/PC-1) PSFs vary significantly with field position due to changes in the obscuration pattern, a result of using small Cassegrain repeater optics to reimaging the telescope's focal plane onto CCDs. Each repeater has a secondary mirror supported by spiders. Because these structures are not located at a pupil their silhouettes, when projected into the exit pupil, appear to shift relative to the telescope's obscurations depending

on field position. At the edges of a WFPC2 detector, the PSF core is significantly elongated due to the large apparent shift between the telescope and repeater secondaries. This makes very-small-aperture photometry or cosmic shear studies extremely difficult in WFPC2. Even small offsets ($\sim 1''$) can alter the PSF enough to affect high-contrast programs that rely on stability for PSF subtraction. Fortunately, ACS uses off-axis optics and does not introduce any additional obscurations, resulting in a much more stable PSF over a larger field.

Charge Diffusion

Another effect, one that has not really been examined closely before, is the field-dependent blurring of the image caused by variations in charge diffusion. In a CCD an electron is generated by the absorption of a photon within the photosensitive (epitaxial) layer. If the electric field is weak at the depth at which the electron is generated, the charge may wander into and be detected within an adjacent pixel. The chance of this occurring increases the further away the electron is generated from the electrodes that define the potential well. The net effect is blurring of the image, so charge diffusion increases the apparent FWHM of the PSF and degrades encircled energies at small radii.

The depth at which a photon is absorbed is proportional to the wavelength. Red photons will travel further into the CCD than blue ones. How the wavelength actually impacts charge diffusion depends on the configuration of the detector. Frontside-illuminated CCDs, like those used in WFPC2, have semi-transparent electrodes on the illuminated side, so charge diffusion is greatest in the red because electrons are generated near the back surface. Conversely, in backside-illuminated chips, like those used in ACS, the electrodes are on the rear face. In this case, blue photons are absorbed close to the illuminated surface, far from the electrodes, and charge diffusion is therefore greater than in the red.

Backside-illuminated CCDs are typically thinned by removing the layer of photo-insensitive material on the surface opposite of the electrodes, exposing the photosensitive epitaxial layer that is 10-20 μm thick. This reduces unproductive absorption of short wavelength photons, improving the quantum efficiency in the blue relative to frontside-illuminated devices (QE is also helped by photons not having to pass through the electrodes). Because the thinning process is inexact, variations in the epitaxial layer thickness will create variable charge diffusion over the area of the detector – thicker regions will suffer greater charge diffusion. At long wavelengths ($>0.8 \mu\text{m}$) photons may pass through the entire CCD layer and be absorbed by the mounting substrate or be reflected back into the epitaxial layer. In the latter case, the photon may be absorbed at nearly any depth, so the variation in charge diffusion with thickness will be less than at shorter wavelengths. A

frontside-illuminated device should not have significant charge diffusion variations because the epitaxial layer behind the electrodes has practically constant thickness.

Charge diffusion was characterized by the ACS IDT at various wavelengths using pinhole spot images for a spare STIS CCD like that used in the HRC (21 μm pixels). The results were extrapolated to the WFC (15 μm pixels). On-orbit comparisons indicate that these pinhole-derived profiles are too sharp, so diffusion is greater than expected in the flight detectors.

Conventions Used In This Report

Aberration values in this document are specified in microns of root-mean-square wavefront error. The coordinate system is defined by the undistorted image X,Y axes with positive angles measured counterclockwise from the +X axis. Note that this is a different coordinate system than is used by the Tiny Tim PSF modeling program.

Focus will occasionally be given in microns of equivalent telescope secondary mirror despace, Δ_{SM} , the default unit for describing telescope time-dependent focus variations. Unless explicitly indicated, however, focus is specified as RMS wavefront error. One micron of secondary motion introduces 0.006 μm RMS of wavefront error.

In color figures, red represents the maximum indicated value. Linear-scale color bars are provided.

Images Used In This Study

A set of images (Table 1) of 47 Tuc were analyzed for PSF characterization. In the WFC, 640 stars were measured in F435W, 1022 in F550M, and 592 in F814W. In the HRC, 77 stars were measured in F550M. Pipeline-produced _crj or _flt files were used without any geometric distortion correction to avoid errors that would be introduced by image interpolation. The median of all focus measurements in each frame is given in Table 1.

Table 1: Images used in this study.

Filename	Camera	Filter	Median Focus (μm RMS)
j8c0a2011_crj	WFC	F435W	-0.041
j8hr01021_crj	WFC	F550M	-0.022
j8hw17p3q_flt	WFC	F814W	-0.005
j8hr01011_crj	HRC	F550M	-0.027

Measurements of Field-Dependent Aberrations and Charge Diffusion

Aberrations and charge diffusion can be derived using phase retrieval methods that iteratively compare computed PSFs to observed ones while optimizing the relevant parameters (focus, coma, astigmatism, blur width, etc.). The STScI phase retrieval software (Krist & Burrows 1995) has been used to determine the aberrations in every HST camera and is regularly applied to monitor telescope focus. The program was modified for ACS to geometrically distort the subsampled model PSF it produces and integrate it onto detector pixels before comparing to the data. This avoids errors that would be introduced using observed undersampled images that were distortion-corrected via interpolation or drizzling. The distorted PSF model is convolved with a 3 x 3 pixel kernel representing wavelength-dependent charge diffusion as derived by the pinhole tests. Initial comparisons revealed that these kernels are too sharp, so the PSF is again convolved with a 3 x 3 Gaussian kernel with an adjustable width.

Stars in WFC and HRC F550M, WFC F435W, and WFC F814W images of 47 Tuc were individually fit by the phase retrieval software. Each fit returned defocus, x and y coma, 0° and 45° astigmatism, x and y center, background, and Gaussian blur width. Because the software generates purely monochromatic PSF models, the values derived for WFC from the medium bandpass F550M image are considered more accurate than those from the broader filters. The aberration variation patterns are similar among the filters and should not be wavelength-dependent, so only the F550M results are presented.

WFC

The measured WFC values are shown relative to field position in Figures 2 & 3. Focus varies by about $\pm 0.015 \mu\text{m}$ over the WFC field of view, which is equivalent to $\Delta_{\text{SM}} = \pm 2.5 \mu\text{m}$ of breathing. It is obvious from the discontinuities in the focus pattern at the chip boundaries that defocus is dominated by surface height variations between and within the detectors rather than by optical effects. The focus between the two CCDs differs by up to $0.02 \mu\text{m}$ along the gap between them, which implies that the surface of WFC2 (the lower detector in the plots) is $\sim 0.4 \text{ mm}$ below that of WFC1 at the maximum offset (note that surface height is not the same as thickness of the epitaxial layer). Because the focus differences are small, they are difficult to visually correlate with the PSF variations seen in Figure 1, except when they interact with astigmatism to produce elongated PSFs near the corners and edges.

In contrast to focus, the other aberrations, coma and astigmatism, are insensitive to chip boundaries and are instead defined by the optical system. Coma is less than $0.015 \mu\text{m}$ over about 90% of the field, with the largest values ($\sim 0.03 \mu\text{m}$) concentrated in the upper

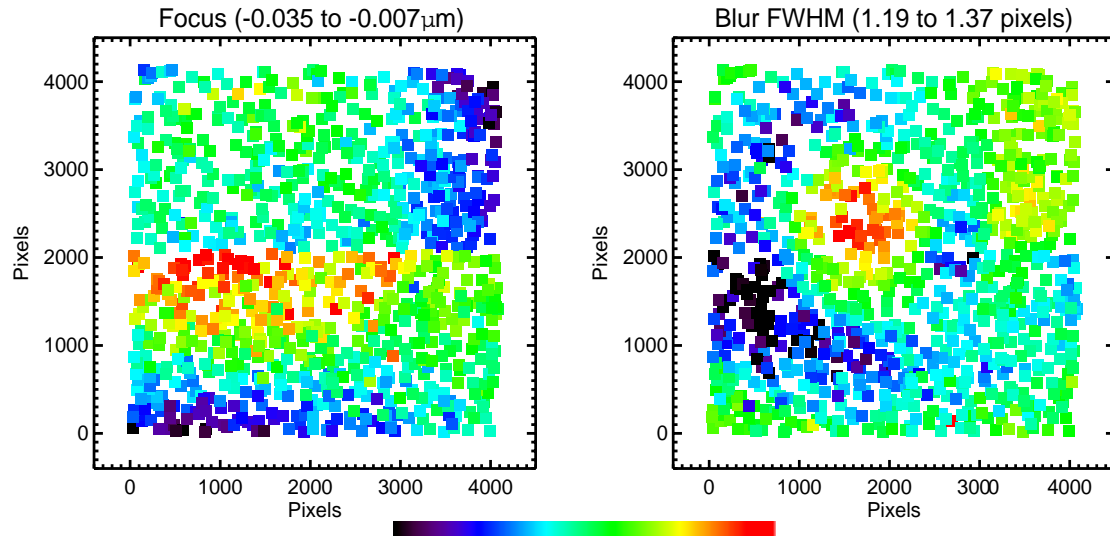


Figure 2: ACS/WFC focus wavefront error variations and charge diffusion blur widths derived from phase retrieval measurements of the F550M image.

left corner. The resulting shift of the PSF centroid in this corner can be seen in the star images in Figure 1. Astigmatism varies by $\sim 0.04 \mu\text{m}$ over the field and is greatest along the left and right edges. This correlates with the elongation of the PSFs in Figure 1, though the interaction of astigmatism and focus enhances the asymmetries in the corners.

The blurring caused by charge diffusion (Figure 2) is greatest within a “hill” near the field center and along the outer field boundaries and is least within a “moat” surrounding the hill. The pattern is continuous across the gap between the two devices, an artifact of the CCDs having been cut from the same thinned wafer. As demonstrated later, this pattern is very similar to measured variations in the CCD thickness. The corresponding best and worst case blur kernels (pinhole-derived charge diffusion kernel convolved with the Gaussian blur kernel) are given in Table 2.

Surface fits to the measured blur values in the three filters are shown in Figure 4. As expected, the largest variations in charge diffusion are seen at the shortest wavelength, where electrons are generated near the top surface of the detector, far from the electrodes. In the best case in F435W, half of the light falling within a pixel is detected in it; in the worst case less than one-third is. The blur is reduced in both variation and strength in the red as electrons are generated near the electrodes at the bottom of the pixel.

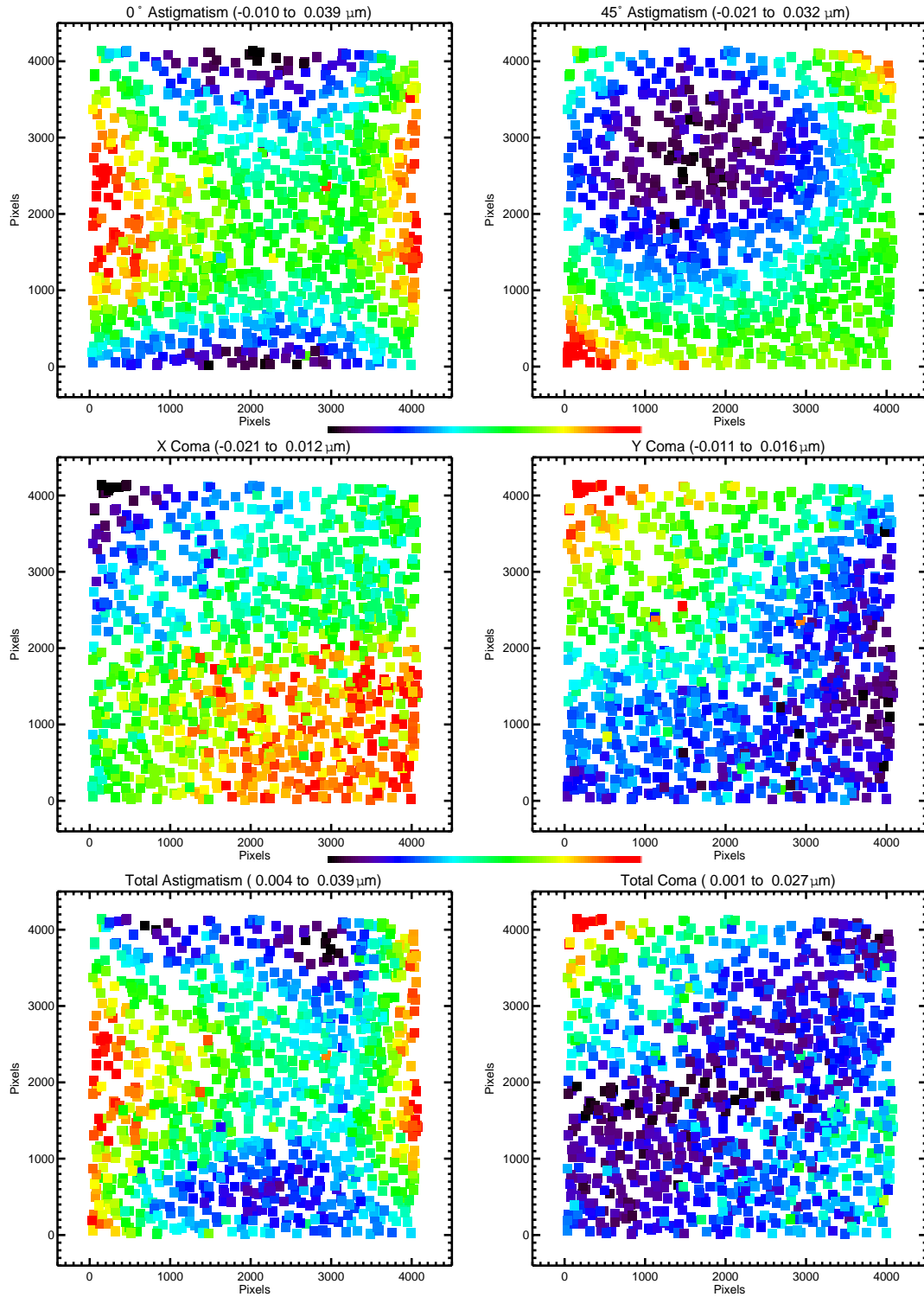
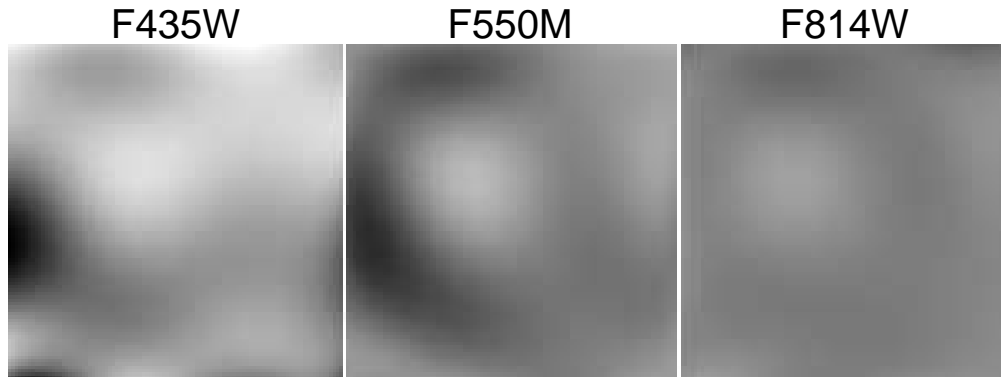


Figure 3: ACS/WFC aberrations derived from the F550M image.

Table 2: ACS/WFC charge diffusion blurring kernels.

	<u>Best Case</u>			<u>Worst Case</u>	
F435W					
0.0312	0.1002	0.0312	0.0561	0.1224	0.0561
0.1002	0.4741	0.1002	0.1224	0.2858	0.1224
0.0312	0.1002	0.0312	0.0561	0.1224	0.0561
F550M					
0.0254	0.0809	0.0254	0.0379	0.1104	0.0379
0.0809	0.5746	0.0809	0.1104	0.4069	0.1104
0.0254	0.0809	0.0254	0.0379	0.1104	0.0379
F814W					
0.0134	0.0536	0.0134	0.0200	0.0866	0.0200
0.0536	0.7318	0.0536	0.0866	0.5735	0.0866
0.0134	0.0536	0.0134	0.0200	0.0866	0.0200

Figure 4: Surface fits to the measured WFC charge diffusion blur kernel widths shown over the entire field of view (WFC1 & WFC2 butted together). The images are scaled to the same linear range.



HRC

The aberration and charge diffusion variations in the HRC are less well defined than in the WFC due to the smaller detector and field of view (Figures 5 & 6). Focus varies by

$\pm 0.005 \mu\text{m}$, the equivalent of $\Delta_{\text{SM}} = \pm 0.9 \mu\text{m}$. Coma variations are less than $\pm 0.004 \mu\text{m}$ with no strong pattern. Astigmatism varies by $\pm 0.01 \mu\text{m}$, which results in no obvious visible effects.

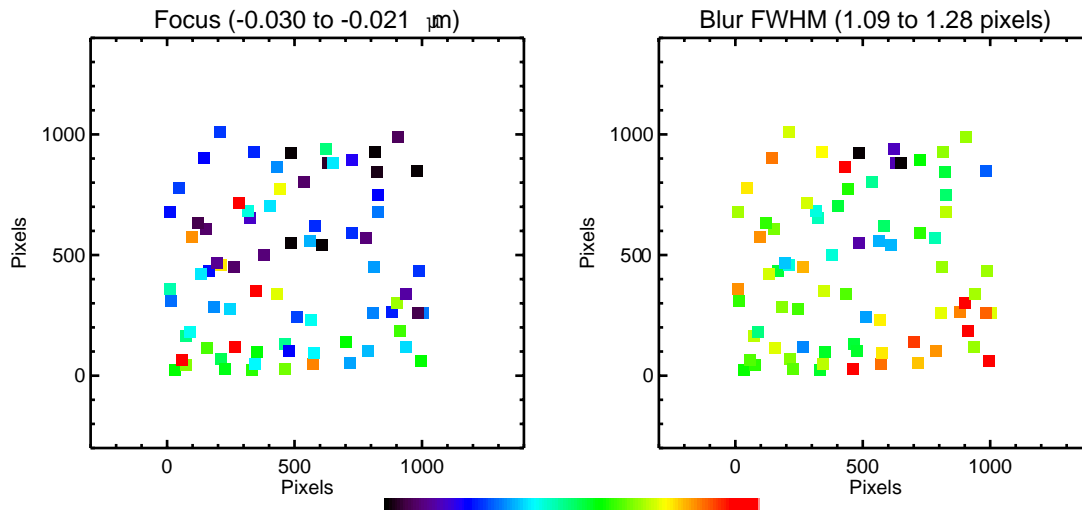
Charge diffusion variations are difficult to measure accurately in the HRC because the PSF is better sampled than in the WFC. However, the variations are clearly small. In the best case 68% of the light falling within a pixel is detected in it, 54% in the worst case (Table 3). Diffusion is greatest in the lower right corner.

Table 3: ACS/HRC charge diffusion blurring kernels.

	Best Case			Worst Case		
F550M						
	0.0185	0.0613	0.0185	0.0243	0.0894	0.0243
	0.0613	0.6806	0.0613	0.0894	0.5452	0.0894
	0.0185	0.0613	0.0185	0.0243	0.0894	0.0243

Given that only an F550M HRC image was measured, the charge diffusion width variations at other wavelengths are unknown but are expected to follow the trend seen in the WFC. The one caveat is that the HRC CCD lacks the metallicized backing present in the WFC detectors that would reflect most of the red photons back into the same pixel.

Figure 5: ACS/HRC focus wavefront error variations and charge diffusion blur widths derived from the F550M image.



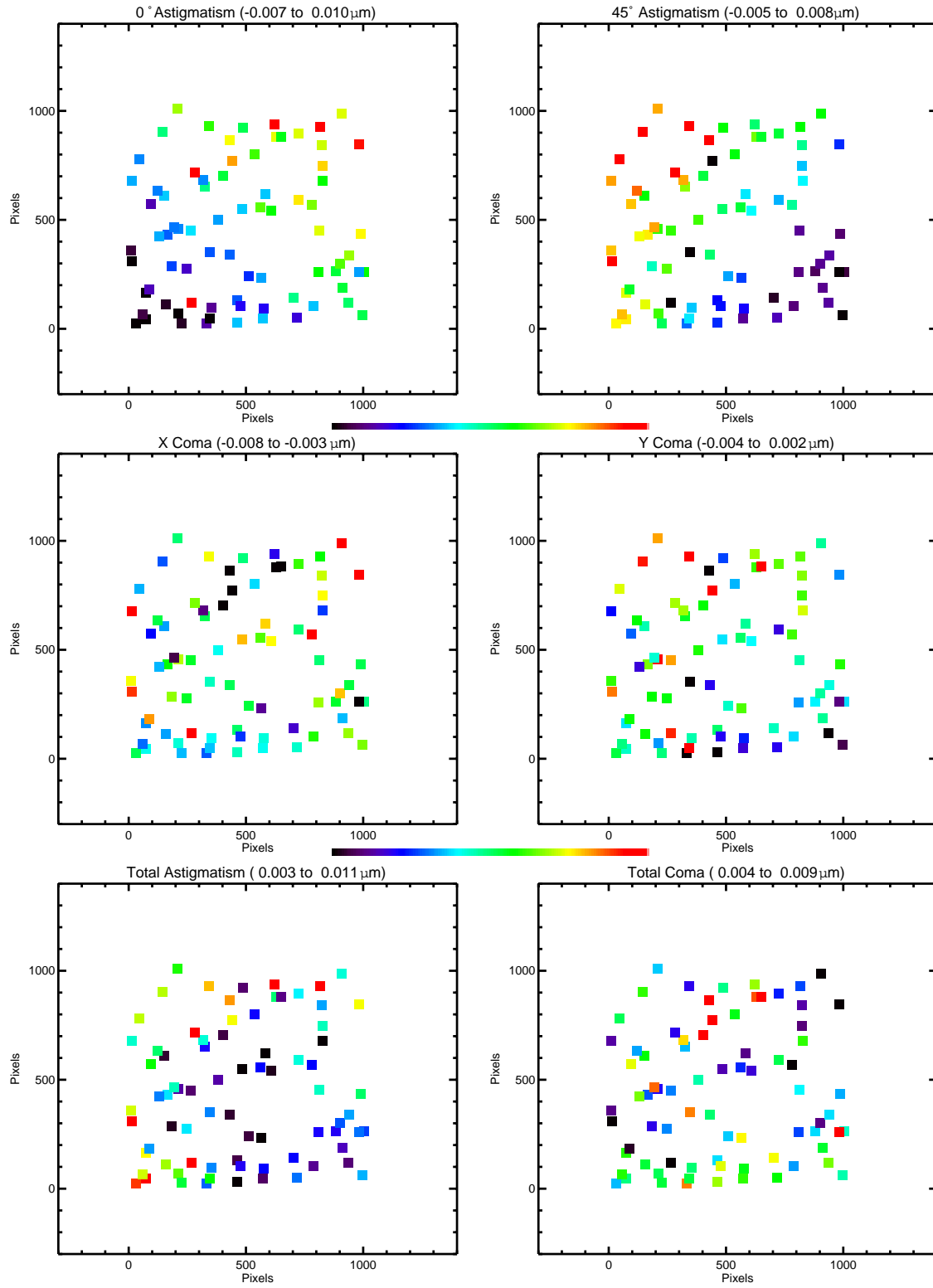


Figure 6: ACS/HRC aberrations derived from the F550M image.

ACS PSF Field Dependence Characterization

The simplest measures of PSF variations over the field are the core major and minor axis FWHMs, the aspect ratio ($a = \text{major/minor axis FWHM}$), and major axis angle (θ). These were derived from the 47 Tuc images using the IRAF task *noao.digiphot.apphot.fitsf*. Note that *fitsf* fits an elliptical Gaussian, which is not exactly the shape of the real PSF. However, it is close enough for the purposes of this study.

Because these characteristics may change with focus, which is a time-dependent quantity, observers may wish to investigate their variation with filter and focus using Tiny Tim models, as demonstrated later.

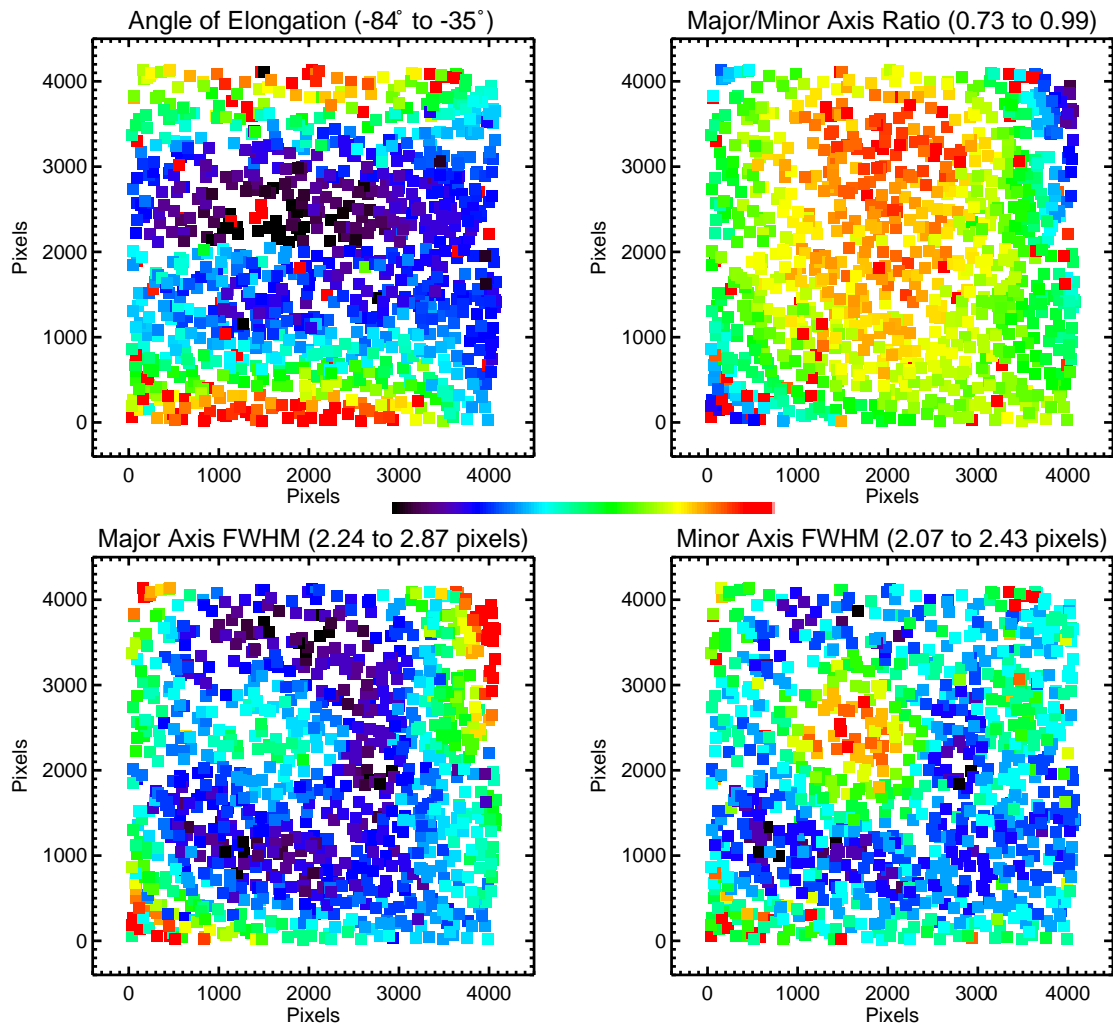


Figure 7: ACS/WFC PSF core characteristics in the F550M image.

WFC

The results for the WFC are shown in Figures 7-9. In F550M, the minor axis FWHM varies between 2.1-2.4 pixels (0.10"-0.12") and the major axis between 2.2-2.9 pixels (0.11"-0.14"). The patterns are similar to the variations in charge diffusion. The minor axis FWHM is largest within the "hill" where charge diffusion is highest and narrower in the "moat" where diffusion is less. The major axis FWHM pattern is similar, though it is enhanced in the corners of the field and is not smoothly continuous across the gap. This correlates with the combined variations in astigmatism and focus seen previously. These results indicate that, in this case, the major axis width is sensitive to both aberrations and diffusion while the minor axis is dominated by diffusion effects. θ varies symmetrically about the horizontal axis, and there is a small discontinuity in the pattern at the gap that is due to the surface height offsets between the two detectors. The PSF becomes more elongated away from the center of the field, as demonstrated in the aspect ratio pattern.

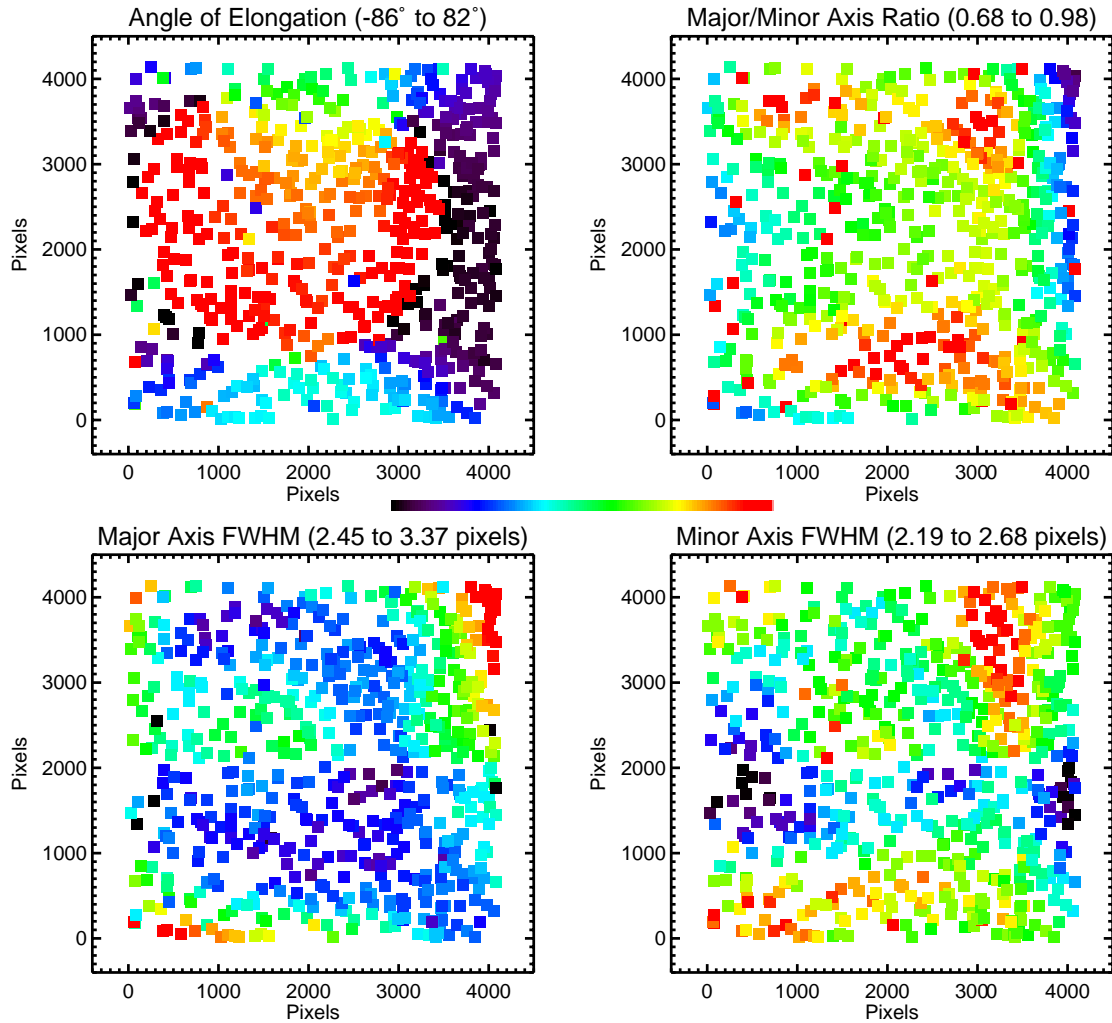


Figure 8: ACS/WFC PSF core characteristics in the F435W image.

In F435W the effects of aberrations are greater due to the shorter wavelength. The PSF variations are more sensitive to aberrations rather than charge diffusion. The minor axis FWHM pattern, for example, shows hints of the astigmatism pattern, and the major axis pattern appears to be an equal mix of aberration and charge diffusion effects. In F814W, on the other hand, the variations are poorly defined as the PSF becomes better sampled relative to the detector and the effects of aberrations are lessened. One caveat regarding these results is that the F435W data was more defocused than F550M, and F814W was more in-focus than either. The combination of defocus and short wavelength therefore accentuates the astigmatism-induced asymmetries in F435W relative to the other filters.

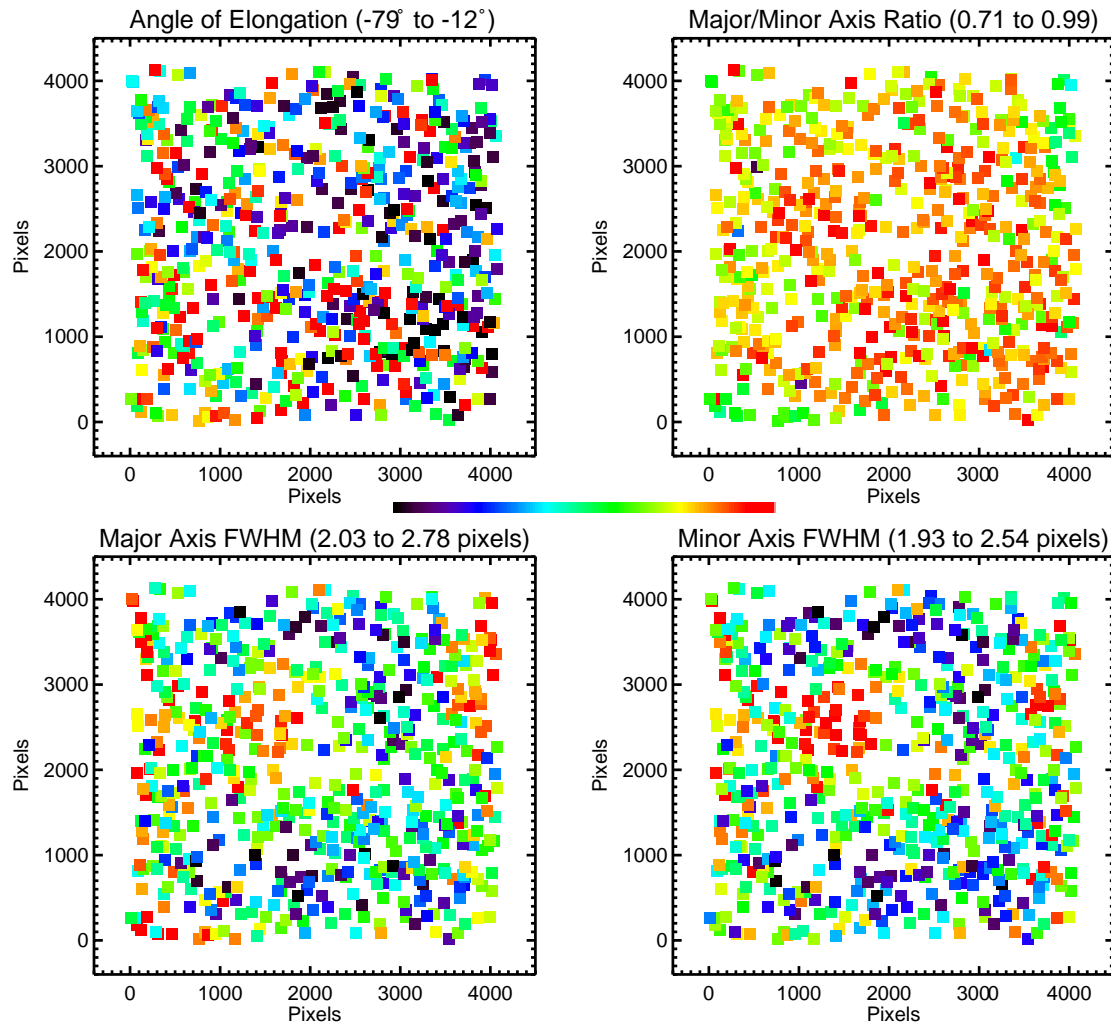


Figure 9: ACS/WFC PSF core characteristics in the F814W image.

HRC

Variations in the HRC measurements are less obvious (Figure 10) because of the smaller field and detector. The major axis FWHM varies between 2.5-2.9 pixels (0.06''-0.07'') and the minor axis between 2.1-2.4 pixels (0.05''-0.06'').

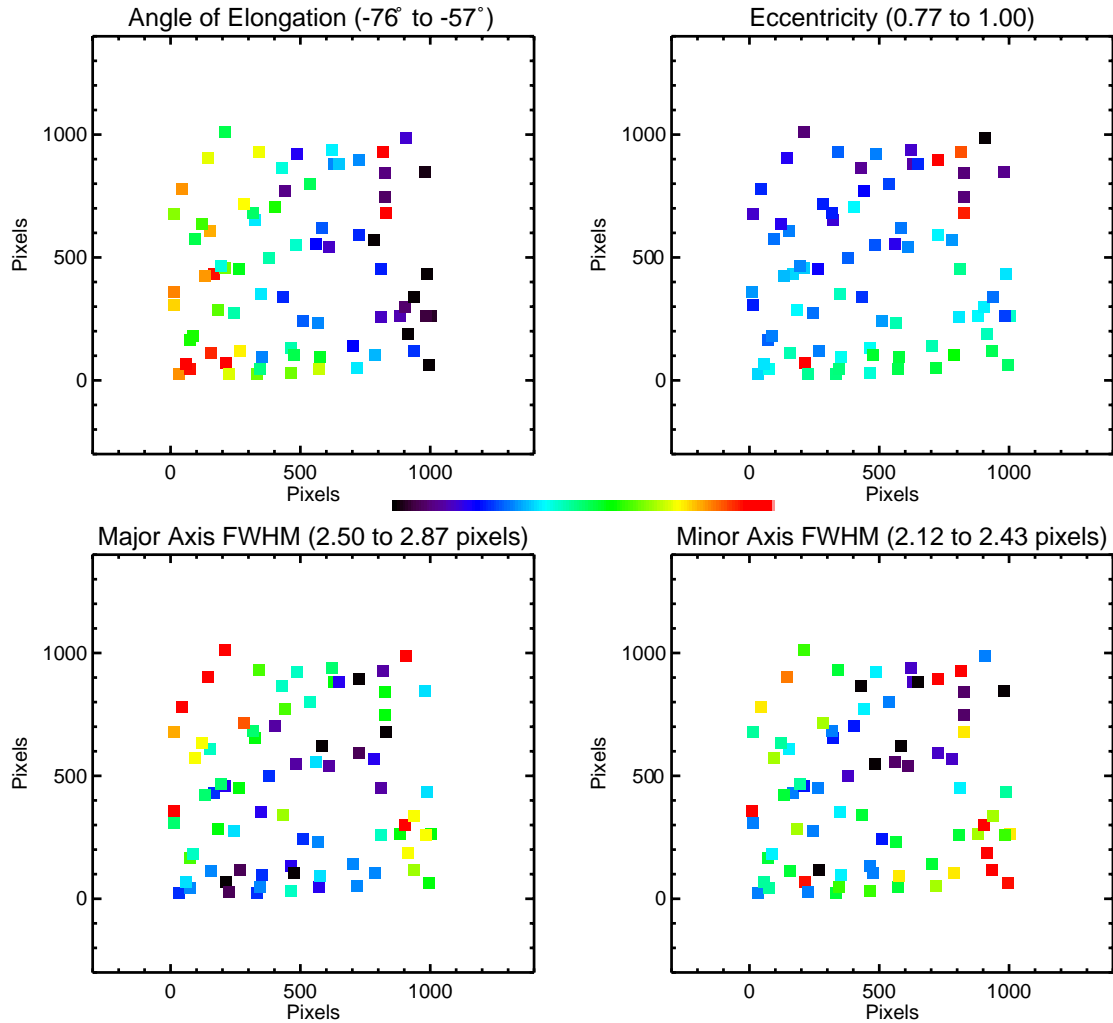


Figure 10: ACS/HRC PSF core characteristics in the F550M image.

The Relationship of Charge Diffusion To Derived CCD Thickness

Thickness variations in the ACS CCDs have recently been derived from fringe flats obtained during ground tests of the cameras (Walsh et al. 2003). These results (Figure 11) show that the primary epitaxial layer thickness varies between 12.6-17.0 μm in the WFC and 12.5-16.0 μm in the HRC. There is a clear correlation between the charge diffusion

(Figure 2) and CCD thickness variation patterns – diffusion is greater in thicker regions of the CCD.

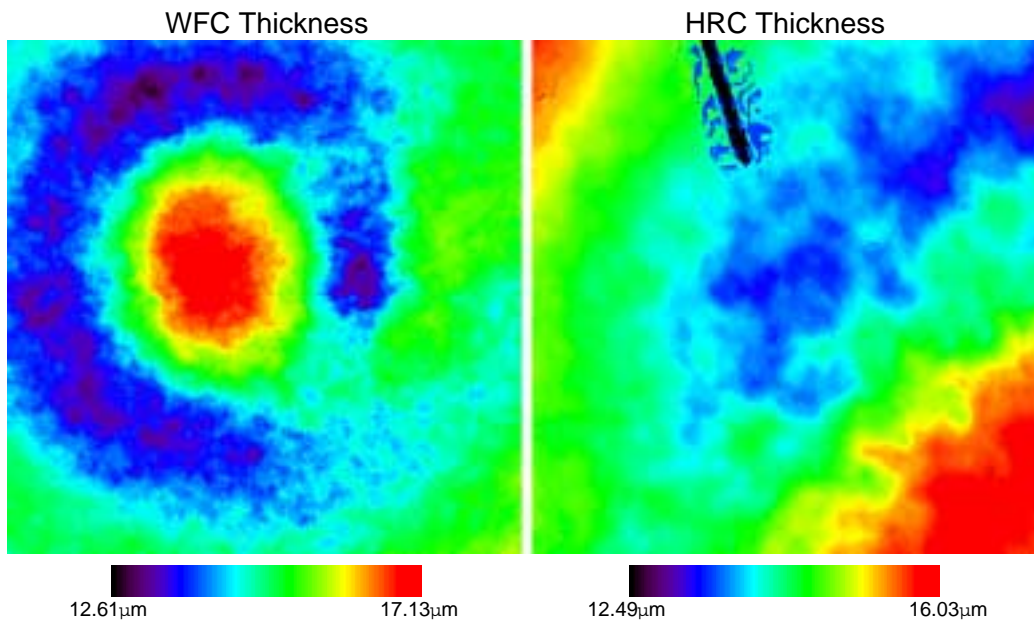


Figure 11: ACS WFC & HRC CCD thicknesses derived from fringe flat modeling (Walsh et al.).

Integration Of Field-Dependence Measurements Into Tiny Tim

Implementation

The measured ACS field-dependent variations in aberrations and charge diffusion widths are included in Tiny Tim version 6.1. The F550M aberration variation patterns were characterized by fitting 5th-order polynomial surfaces to the measurements. The focus pattern for each WFC chip was fit separately. An aberration surface is defined relative to the mean value within a 10" radius of the field center in the WFC and 5" radius in the HRC. The WFC F435W, F550M, and F814W charge diffusion width variation patterns were also fit, producing separate variation maps to account for wavelength dependences. Due to the scatter in the HRC charge diffusion pattern, the CCD thickness map of Walsh et al. was scaled to reasonably fit the measurements, and the polynomial surface was fit to it instead.

By default Tiny Tim assumes that the HRC is at perfect focus. WFC2 is offset from WFC1 by +0.02 μm at the WFC field center. Both are offset from the HRC by an additional +0.015 μm at the field center), based on focus-monitoring program results. The user can alter the focus values by changing the appropriate parameter in the file produced by *tiny1*, but care must be taken that the same offset is applied to both WFC channels.

Tiny Tim asks the user for the X and Y pixel coordinates of the PSF being modeled. From those, the appropriate aberrations and blur widths are computed. A subsampled, polychromatic PSF is computed by *tiny2* which is then integrated onto geometrically-distorted, detector-sized pixels by *tiny3*. The distorted PSF is then convolved with the 3 x 3 charge diffusion kernel derived from the pinhole measurements and then by a 3 x 3 Gaussian kernel representing the additional field-dependent charge diffusion derived in this study. Both kernels are generated for the wavelength of the PSF by interpolating between the wavelengths at which the charge diffusion fits are defined. For a polychromatic PSF, bandpass-weighted-mean kernels are used.

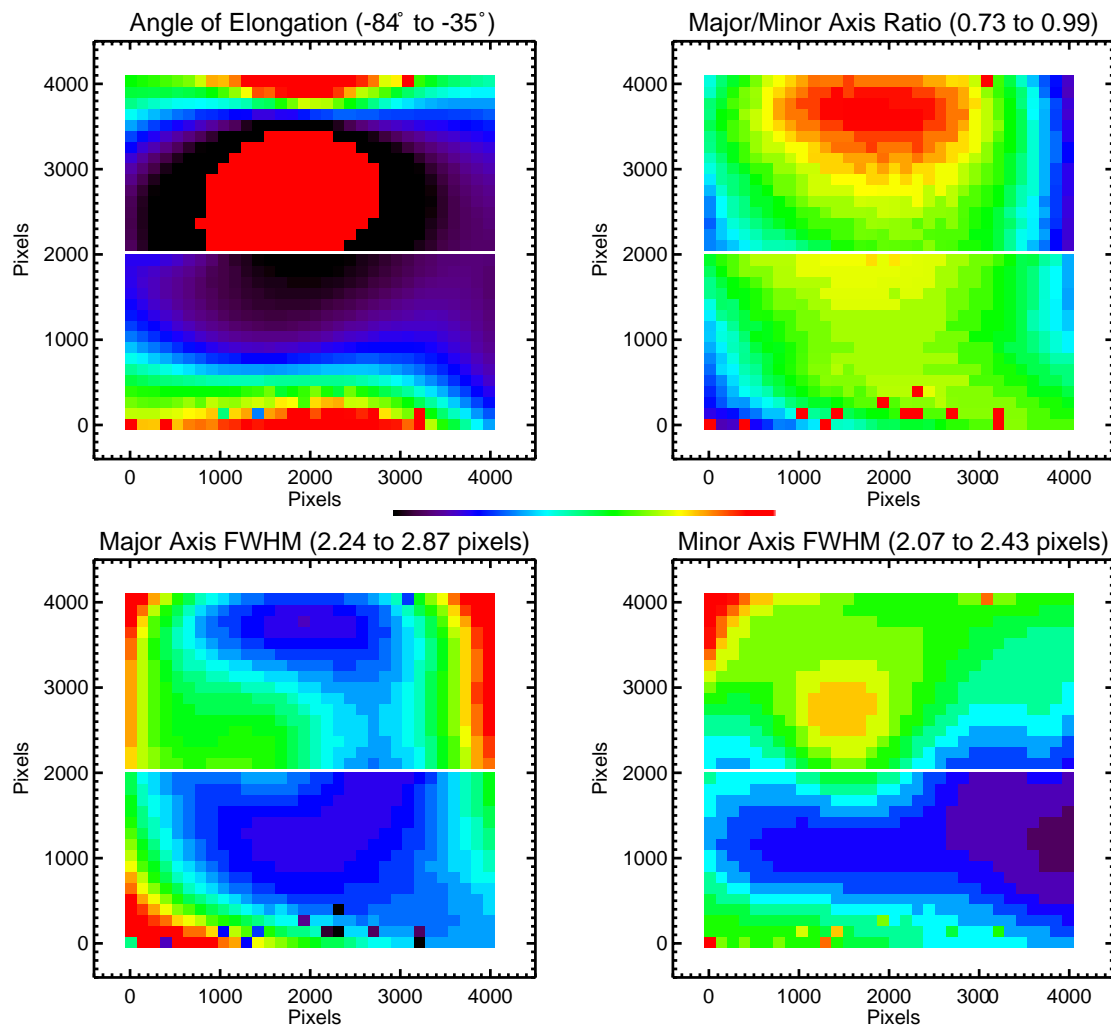


Figure 12: Measured variations in Tiny Tim model PSF characteristics for WFC F550M. The general focus offset was set to match the F550M 47 Tuc image. The central red region in the elongation angle plot is caused by the angle dipping below -90° and wrapping to 90° . These patterns match the observed ones (Figure 7).

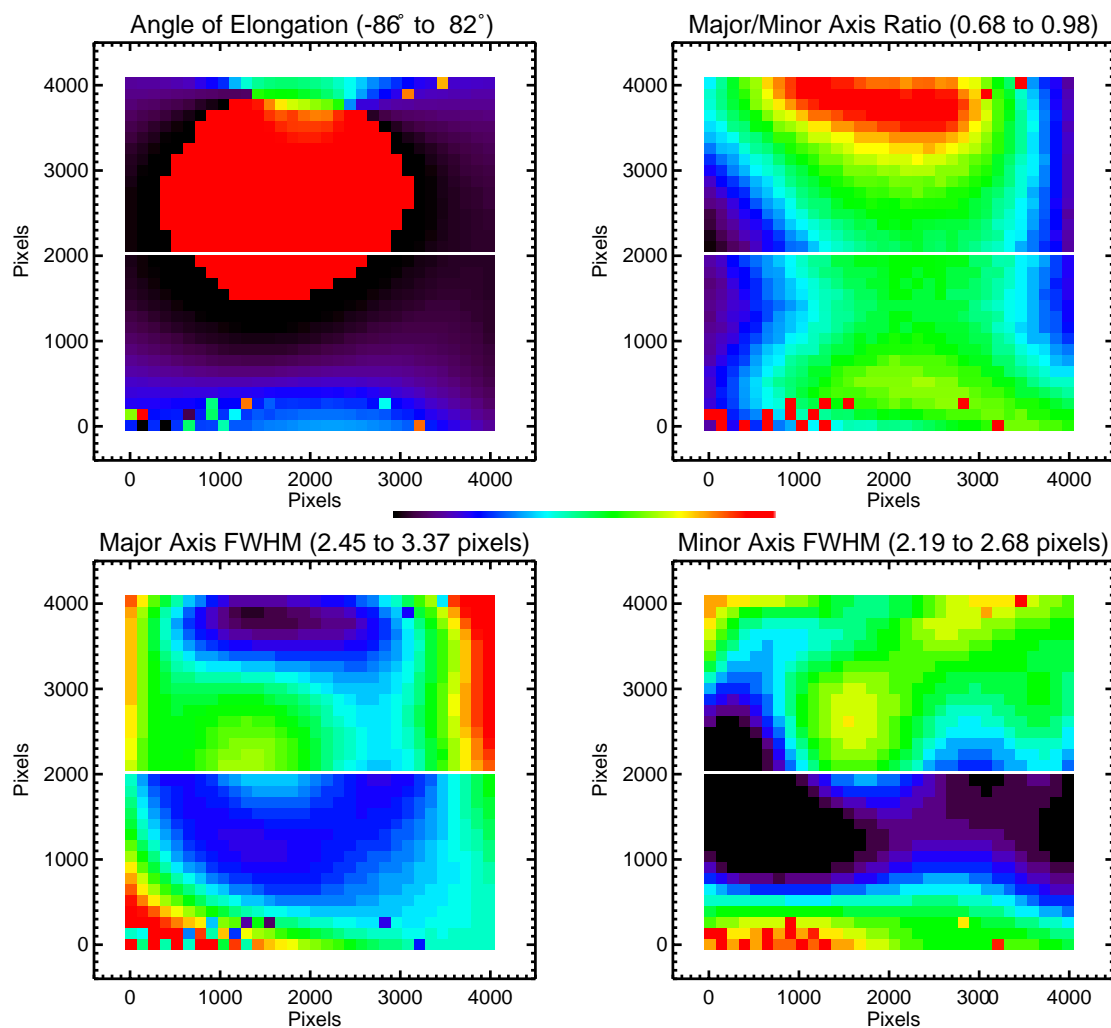


Figure 13: Measured variations in Tiny Tim model PSFs for WFC F435W. The general focus offset was set to match the F435W 47 Tuc image. The large central red region in the angle of elongation map is caused by the angle dipping below -90° and wrapping to 90° . These patterns match the observed ones (Figure 8).

Verification

Tiny Tim PSFs were generated on a grid sampling the WFC field in F550M and F435W. The WFC1 and WFC2 default field-center focus settings in the *tiny1*-produced parameter file were adjusted to match those measured in the on-orbit images discussed above. The FWHM of each geometrically-distorted PSF were then measured with *fitpsf*. These measurements do not provide a fully independent verification of the model quality, as the parameters used by Tiny Tim were derived from the images to which the models are compared. However, they should indicate the general level of agreement that may be expected assuming that the focus parameter is optimized by the user for a particular observation.

Also, the aberrations were derived at F550M, so their application at F435W is an independent test.

Because the phase retrieval software generates a monochromatic model and the data is polychromatic, the amount of blur may have been overestimated because of red wavelengths (larger PSF) in the passband that are not included in the model. The models produced by Tiny Tim properly account for the bandwidth of the filter and so should produce results closer to reality. Therefore, global adjustments to the width of the Gaussian charge diffusion kernel were made until the model FWHM values matched those of the data. The Gaussian kernel width derived from phase retrieval was reduced by 10% at 0.55 μm and by 5% at 0.435 μm . These corrections have been implemented in the released version of the software, and the kernels provided earlier in this document reflect the adjustments.

The PSF characteristic measured from the simulated images are shown in Figures 12 and 13 and can be compared to the corresponding observed values given in Figures 7 and 8. The observed and modeled patterns agree well in F550M. In F435W, there are some differences due to slight mismatches in the aberration patterns and the sensitivity of the PSF to these errors at shorter wavelengths.

PSF Variations Predicted by Models

The charge diffusion and aberration variation patterns do not vary with time, but the general focus offset does. Given the interaction of the aberrations with focus, the PSF cannot be fully characterized from a limited number of on-orbit measurements that sample random states of the telescope focus (which can range from $\Delta_{\text{SM}} = 3\text{-}5\text{ }\mu\text{m}$ within an orbit). Therefore, it is useful to explore the impact of these parameters using PSF models.

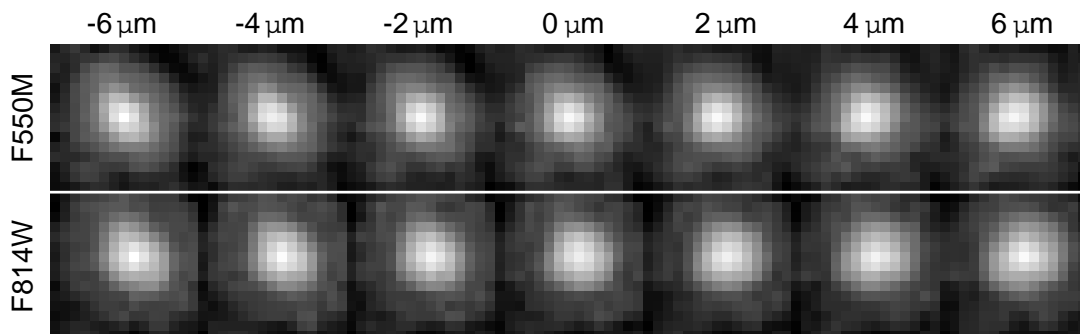


Figure 14: Tiny Tim PSF models at $(x,y)=(100,100)$ on WFC2 illustrating the change in PSF elongation due to astigmatism over a range of focus values. Focus is specified in units of secondary mirror despace.

PSF Elongation and Astigmatism

The most obvious change in the PSF with respect to focus is the amount and angle of elongation due to astigmatism. Figure 14 shows how the PSF varies with focus in the extreme lower left corner of the WFC field. At negative focus values, the PSF core is elongated from the upper-left to lower-right. On the opposite side of focus, the elongation switches by 90° . The asymmetry is difficult to see when the system is within $2\ \mu\text{m}$ of best focus. At shorter wavelengths, the elongation is more pronounced because the wavefront error is greater.

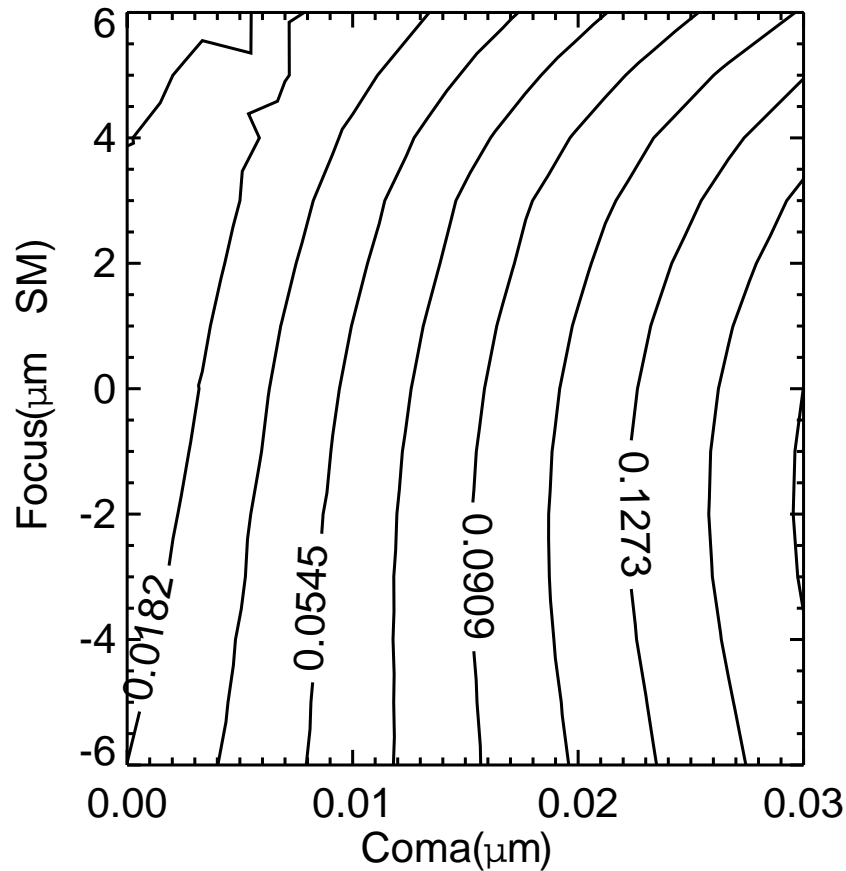


Figure 15: Contours indicating the offset (in WFC pixels) of the measured model PSF center from the true PSF center for WFC F550M with varying amounts of coma and defocus. Focus is specified in units of secondary mirror despace. The contours are not symmetrical about focus due to the presence of other aberrations.

Centroid Offsets and Coma

Changes in the PSF due to small coma variations are not readily apparent, but reveal themselves as shifts in the centroid. To quantify this effect, Tiny Tim WFC F550M models were generated for various amounts of defocus and coma and their centroids measured using both 2-D Gaussian and coma-free PSF model fitting. The latter method involves shifting a subsampled, geometrically-distorted model PSF via cubic convolution interpolation, rebinning it to normal pixel sampling, convolving the result with an appropriate charge diffusion kernel, and comparing it to the data, all in an iterative, optimizing loop. The comatic models always have the true center (where the center of a non-comatic PSF would be) at the center of the same pixel.

The results of the PSF model-fitting procedure are shown in Figure 15. The contours are not symmetric about best focus because of the interaction of focus with other aberrations in the system. As previously noted, coma varies by about $0.015\text{ }\mu\text{m}$ over 90% of the field, which implies that offsets in the measured PSF centers are less than 0.1 pixel ($<0.005''$). Only in the very upper left corner of the WFC field is coma large enough ($\sim 0.03\text{ }\mu\text{m}$) to increase the errors to ~ 0.16 pixel. 2-D Gaussian fits returned offsets $\sim 2.5\times$ larger than those from PSF model fitting. Note that these simulations are for F550M only; the errors will be larger at shorter wavelengths and smaller at longer ones.

Small Aperture Errors

Small aperture (<4 pixels radius) photometry of undersampled data can suffer from errors caused by variations in the width of the PSF over the field. The same grid of WFC F550M model PSFs used to verify Tiny Tim was measured using circular apertures of 1-4 pixels in radius. As shown in Figure 16, the flux within a 1 pixel radius can vary between 85%-106% of the median value over the field, varying in proportion to charge diffusion. In a 2 pixel radius, the range is 93%-102% of the median, and it improves to less than a 1.5% variation at 4 pixels radius. These results are valid only for F550M and will be worse at shorter wavelengths as the PSF becomes even more undersampled and charge diffusion increases.

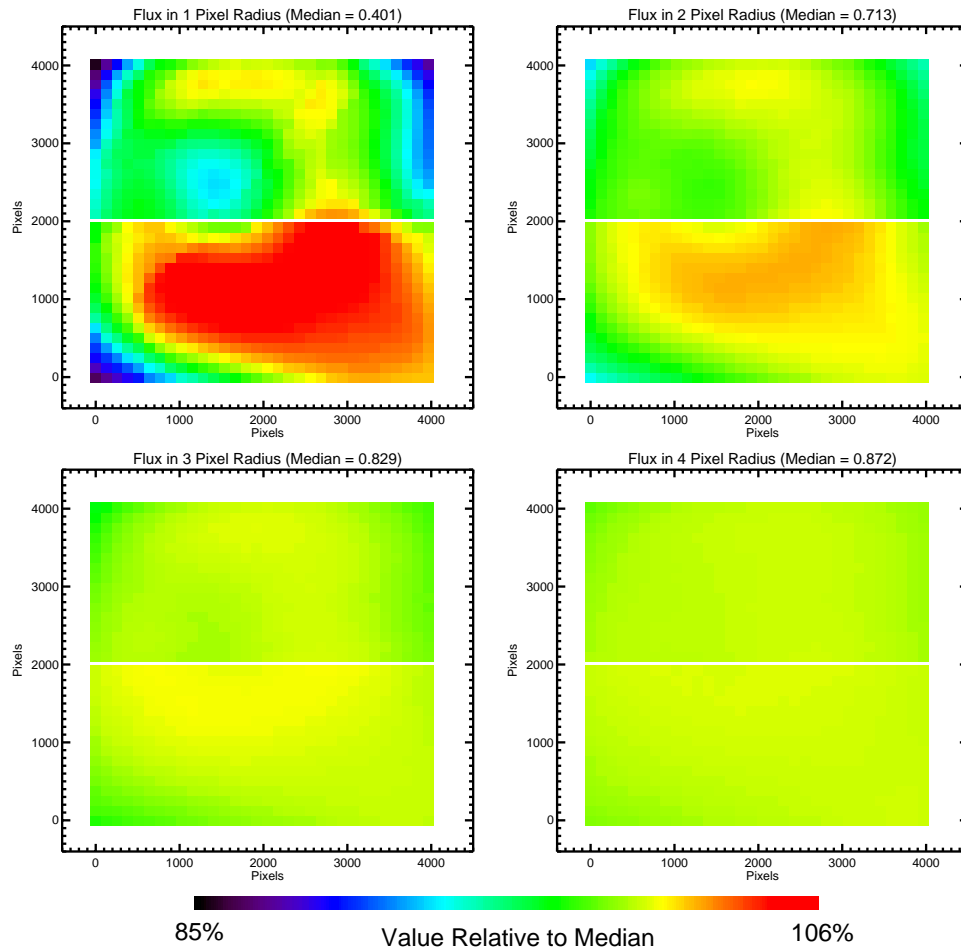


Figure 16: Encircled energies within specified small apertures for WFC F550M, relative to the median value over the entire field.

Conclusions

PSF asymmetry variations over the ACS WFC and HRC fields are caused by optically-induced changes in astigmatism and coma, combined with field- and time-dependent focus variations. In the WFC, surface height variations and offsets between the two detectors dominate the focus changes. For nearly all science programs, coma is negligible except in the extreme upper left of the WFC field, where centroid errors of ~ 0.16 pixels may be expected. Elongation of the PSF is seen in the extreme corners and left and right sides of the field, where astigmatism and focus are relatively large. In the much smaller field of the HRC, the PSF can be essentially regarded as constant.

The minimum width of the PSF core is limited by charge diffusion in the CCD pixels. Due to thickness variations in the detectors, the blurring caused by diffusion alters the PSF FWHM over the field. In the HRC, charge diffusion variation is small, but it is significant in the WFC. There the maximum PSF width is defined by the combined astigmatism and focus wavefront errors, which vary over the field as previously described. Simulations show that the changes in the PSF width due to field- and focus-dependent variations can cause significant errors in photometry when apertures smaller than 4 pixels in radius are used at $\lambda=550$ nm.

Acknowledgements

The author thanks Tom Brown (STScI) for bringing the field-dependent variations to his attention.

References

- Krist, J. & Burrows, C. (1995) *Applied Optics*, 34, 4951
- Meuer, G.R., Lindler, D., Blakeslee, J.P., Cox, C., Martel, A.R., Tran, H.D., Bouwens, R.J., Ford, H.C., Clampin, M., Hartig, G.F., Sirianni, M., and de Marchi, G. (2002) “Calibration of Geometric Distortion in the ACS Detectors” in *Proceedings of the 2002 HST Calibration Workshop*, eds. S. Arribas, A. Koekemoer, & B. Whitmore (STScI)
- Walsh, J.R., Pirzkal, N., & Pasquali, A. (2002) “Modelling the Fringing of the ACS CCD Detectors” in *Proceedings of the 2002 HST Calibration Workshop*, eds. S. Arribas, A. Koekemoer, & B. Whitmore (STScI)

Appendix

The relationship of flat field and CCD thickness variations

The variations in CCD thickness shown in Figure 11 closely resemble the ACS flat field patterns (Figures 17 and 18), which map the effective quantum efficiency (QE) of the detector (ignoring optical effects such as scale distortion and dust specks). At wavelengths below ~ 700 nm, QE is inversely proportional to the CCD thickness - it is high where the chip is thin and low where it is thick. This may indicate the incomplete removal of “dead” material in the thicker regions of the chip during the thinning process. Unproductive absorption of short wavelength photons would lower the QE in these areas. As the wavelength increases, a larger fraction of photons are absorbed deeper in the CCD. At ~ 700 nm, photons can pass completely through the detector and are reflected or scattered back into the device by the back side. This increases the path length and thus chances for productive absorption. In F755W, QE is relatively uniform over the field because the thickness variations are a small fraction of the absorption path length. At long wavelengths, however, the pattern seen in the blue inverts, so that thin regions have the lowest relative QE. Here, the path length is insufficient to absorb all of the photons, some of which are reflected off the backside of the CCD and out of the front of the detector.

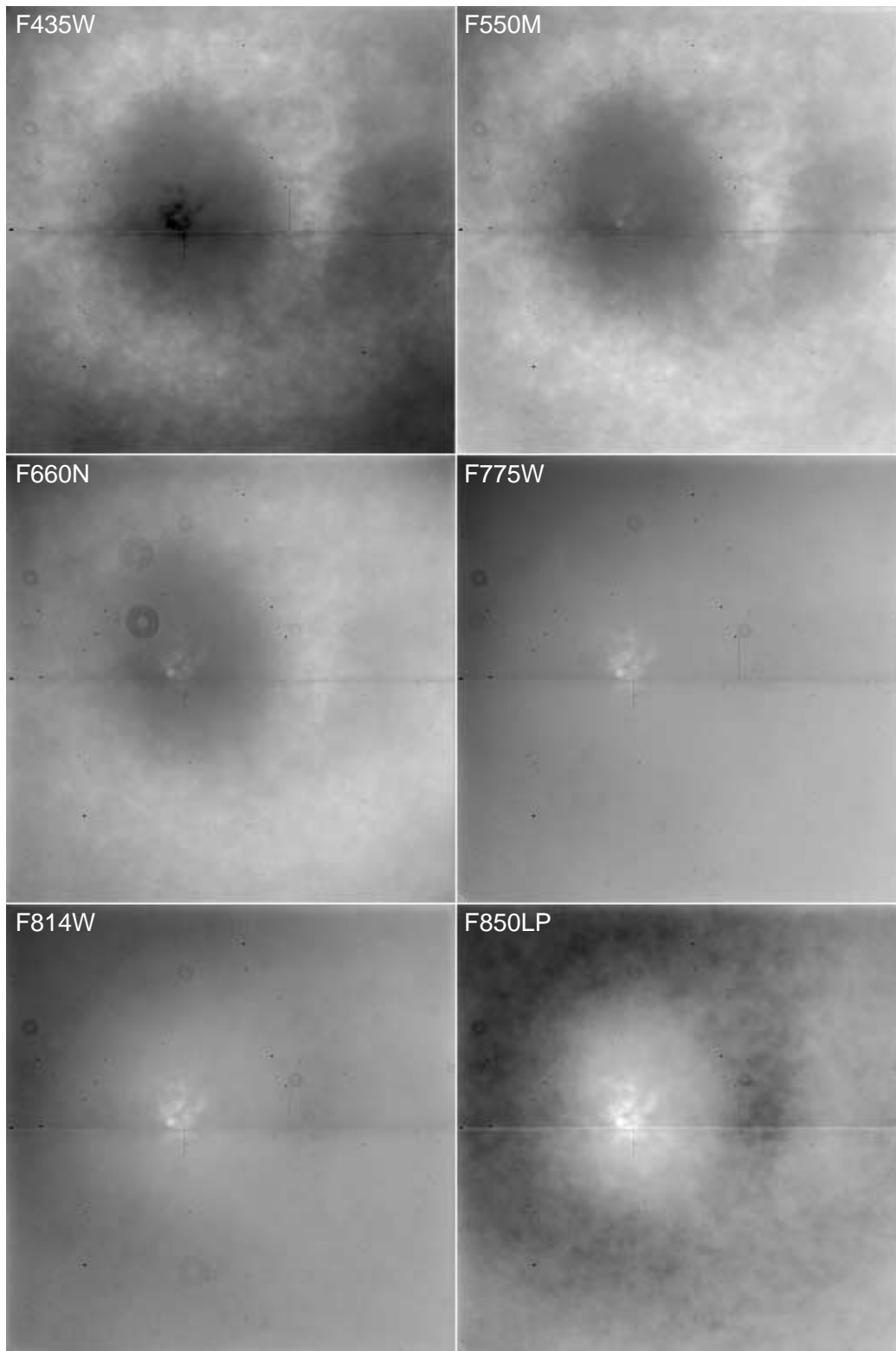


Figure 17: ACS/WFC on-orbit flat fields. Dark areas indicate low effective quantum efficiency. Plate scale variations have been removed.

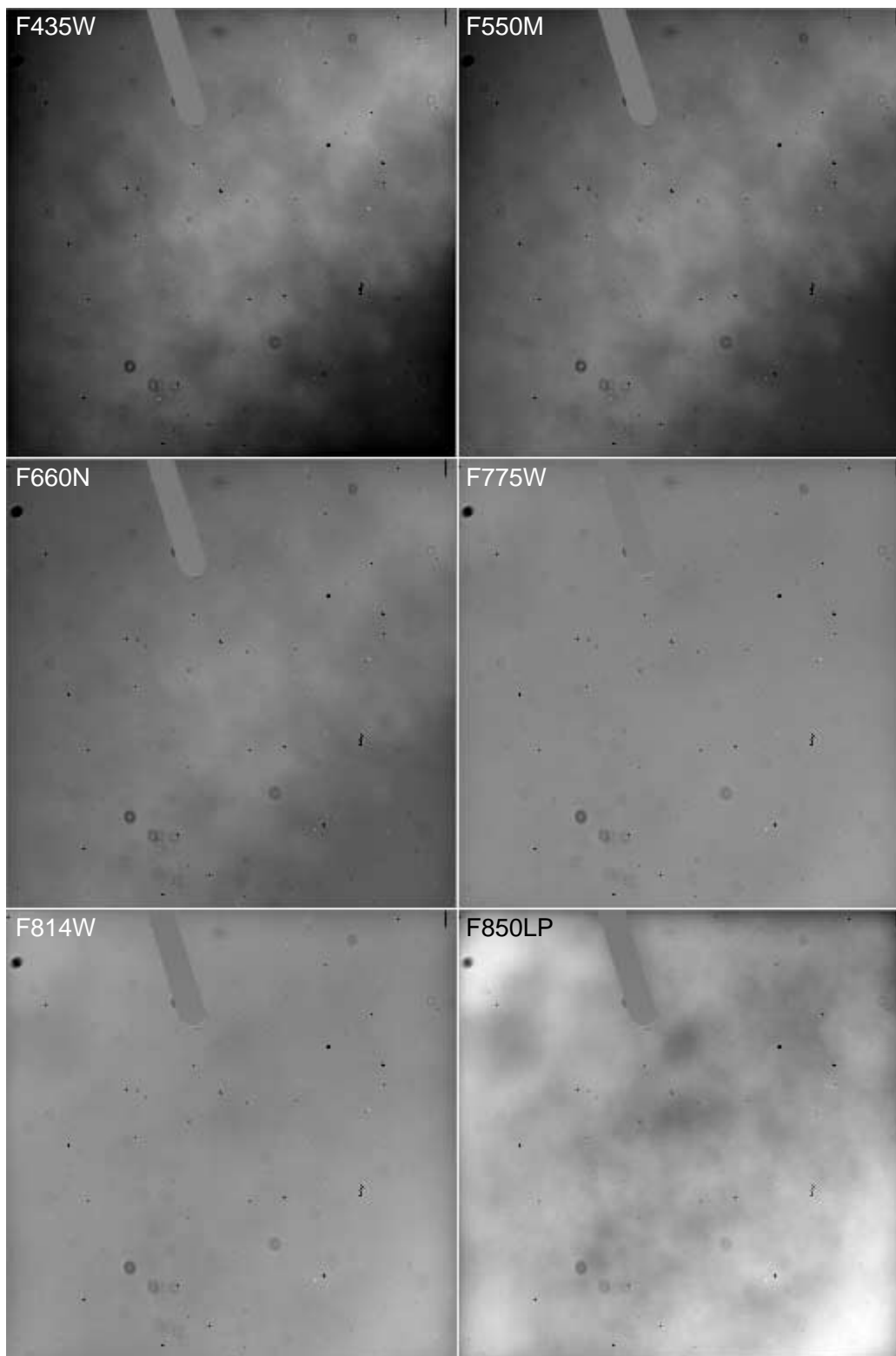


Figure 18: ACS/HRC flat fields.